The 19th Cambridge Workshop on Cool Stars, Stellar Systems, and the Sun
Edited by G. A. Feiden

Photospheric acne at the bottom of the main-sequence: Doppler images of M4.5 - M9V stars

John R. Barnes,[1] Carole A. Haswell,[1] Sandra V. Jeffers,[2] Hugh. R. A. Jones, [3] Yakiv V. Pavlenko, [4] Marcus E. Lohr, [1] James S. Jenkins, [5]

[1] Department of Physical Sciences, The Open University, Walton Hall, Milton Keynes. MK7 6AA. UK (john.barnes@open.ac.uk)
[2] Institut für Astrophysik, Georg-August-Universität, Friedrich-Hund-Platz 1, D-37077 Göttingen. Germany
[3] Centre for Astrophysics Research, University of Hertfordshire, College Lane, Hatfield. AL10 9AB. UK
[4] Main Astronomical Observatory of the National Academy of Sciences of Ukraine, Golosiiv Woods, Kyiv-127, 03680. Ukraine
[5] Departamento de Astronomía, Universidad de Chile, Camino del Observatorio 1515, Las Condes, Santiago. Chile

Abstract

Starspots are an important manifestation of stellar activity and yet their distribution patterns on the lowest mass stars is not well known. Time series spectra of fully convective M dwarfs taken in the red-optical with UVES reveal numerous line profile distortions which are interpreted as starspots. New Doppler images of HU Del (GJ 791.2A; M4.5V), BL Ceti (GJ 65A; M5.5V) and UV Ceti (GJ 65B; M6V) at two epochs separated by three nights are presented. We find that contrast ratios corresponding to photosphere-spot temperature differences of only 100-400 K are sufficient to model the time series spectra of M4.5V - M9V stars. Starspots are reconstructed at a range of phases and latitudes with mean spot filling factors of only a few per cent. The distribution and low-contrast of the spots/spot-groups that we recover are likely to be responsible for the low amplitude photometric variability seen in late-M dwarfs. The stability of the spot patterns in the two sets of timeseries observations enables us to measure the latitude dependent differential rotation, which we find to be consistent with zero.

1 Introduction

Activity indicators have revealed that fully convective M dwarfs possess significant magnetic fields, even though the form of the dynamo mechanism that amplifies the fields remains unclear. Compared with G and K dwarfs, magnetic fields on on M dwarfs have been shown to be very large at 2 - 4 kG (Saar & Linsky 1985; Johns-Krull & Valenti 1996), while more recent techniques[1] have suggested that field strengths may be even greater. Zeeman Doppler imaging using Stokes V observations to probe magnetic field topology have revealed axisymmetric large-scale poloidal fields at the M4V fully convective boundary (Morin *et al.*, 2008a). For M5 - M8V stars, strongly axisymmetric dipolar fields or weak fields with a significant non-axisymmetric component are found.

The majority of mid-late M stars targeted with Stokes V observations did not possess the rotation rates necessary for brightness imaging, enabling the distribution of starspot features to be studied. Only a handful of brightness maps of M dwarfs have been derived using Doppler imaging. Barnes & Collier Cameron (2001) and Barnes *et al.* (2004) studied starspot distributions and differential rotation on early, M1 - M2V stars that are still expected to possess a tachocline, revealing spots distributed across the stellar photospheres. Images of M4V stars at the fully convective boundary have instead revealed fewer spots and lower spot filling factors (Morin *et al.* 2008b; Phan-Bao *et al.* 2009). More recently Barnes *et al.* (2015) studied two mid-late M dwarfs (HU Del; M4.5V and LP 944-20; M9V) revealing a decrease in photosphere-spot contrast, and reduction in starspot coverage with decreasing mass or temperature. Here we present further observations of the M4.5V star studied in Barnes *et al.* (2015), and new images of both components of the nearby visual binary, GJ 65.

[1] D. Shulyak, these proceedings

2 Observations

Observations were made with UVES at the VLT on 2015 September 25/26 & 28/29. HU Del (GJ 791.2A) was observed during the first half of each night. During the second half of the night, both components of GJ 65, were observed together on the slit. In 2015, BL Ceti (GJ 65A; M5.5V) and UV Ceti (GJ 65B; M5.5V) were separated by $2.15''$. Because favourable seeing conditions of typically $< 1''$ prevailed on both nights, we were able to place both components on the spectrograph slit and observe them simultaneously. Frame-by-frame examination of the cross-dispersion profiles of each star enabled the the spectra to be extracted without cross-contamination. A total of 86 and 77 spectra of HU Del were obtained on each respective night using 180 sec exposures. For BL Ceti and UV Ceti, 91 and 87 spectra with 180 sec exposures were obtained. The observations were made with a $0.4''$ slit (R $\sim$ 100,000) in the red-optical, with a spectral range of 0.645 μm - 1.025 μm.

3 Imaging methods

Using empirical line lists derived from slowly rotating standard stars, we applied our implementation (Barnes *et al.*, 1998, 2012) of the least squares deconvolution (LSD) algorithm first described by Donati *et al.* (1997). This enables

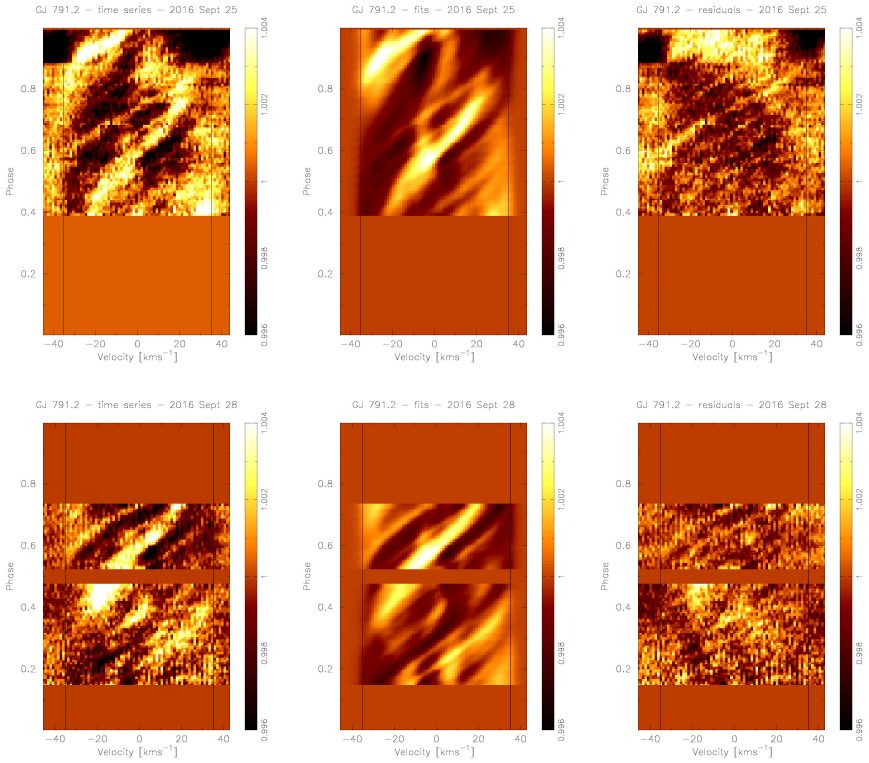

Figure 1: Phased residual spectral time series spectra of HU Del (GJ 791.2A; M4.5V). The deconvolved spectral profiles have been divided by the mean profile; starspot trails appear white. The vertical lines denote the v sin i = 35.3 kms^{-1}.

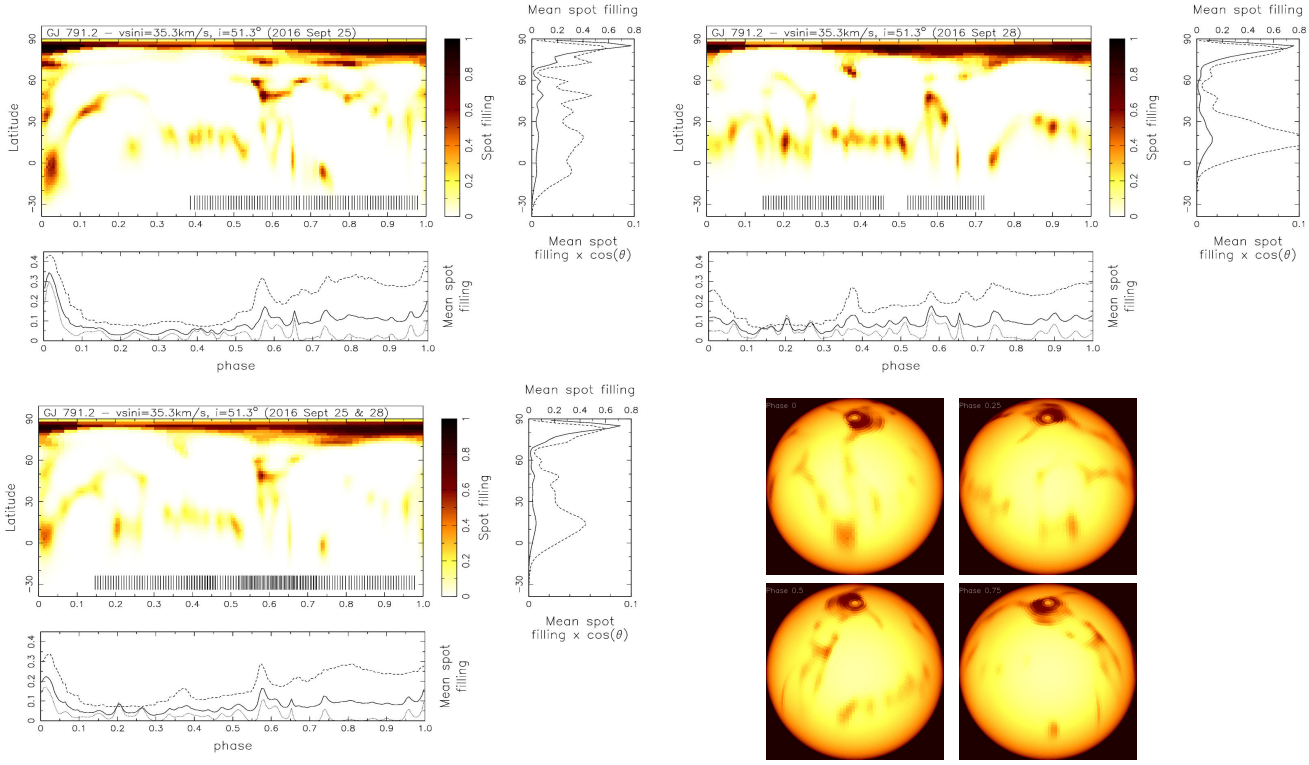

Figure 2: Mercator projection images of HU Del for 2015 August 25 and 28 (top left & right) and both nights combined (bottom left). Tick marks indicate the observation phases. 3D representation for both nights combined (bottom right), showing phases 0.00, 0.25, 0.50 & 0.75 (top-left to bottom-right).

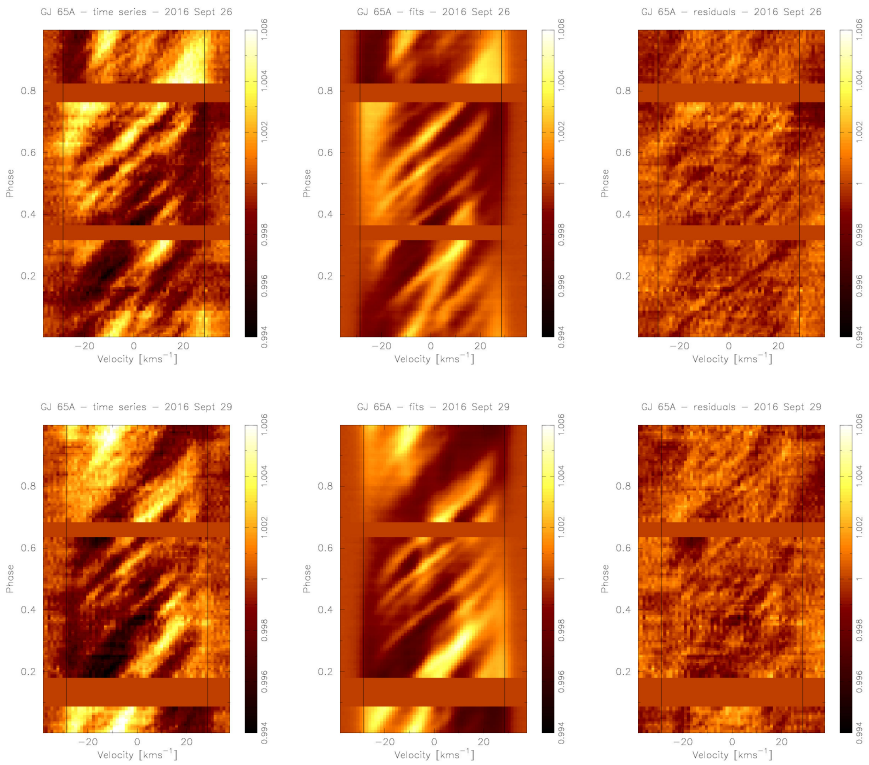

Figure 3: As in Fig. 1 for BL Ceti (GJ 65A; M5.5V). v sin i = 28.6 kms^{-1}.

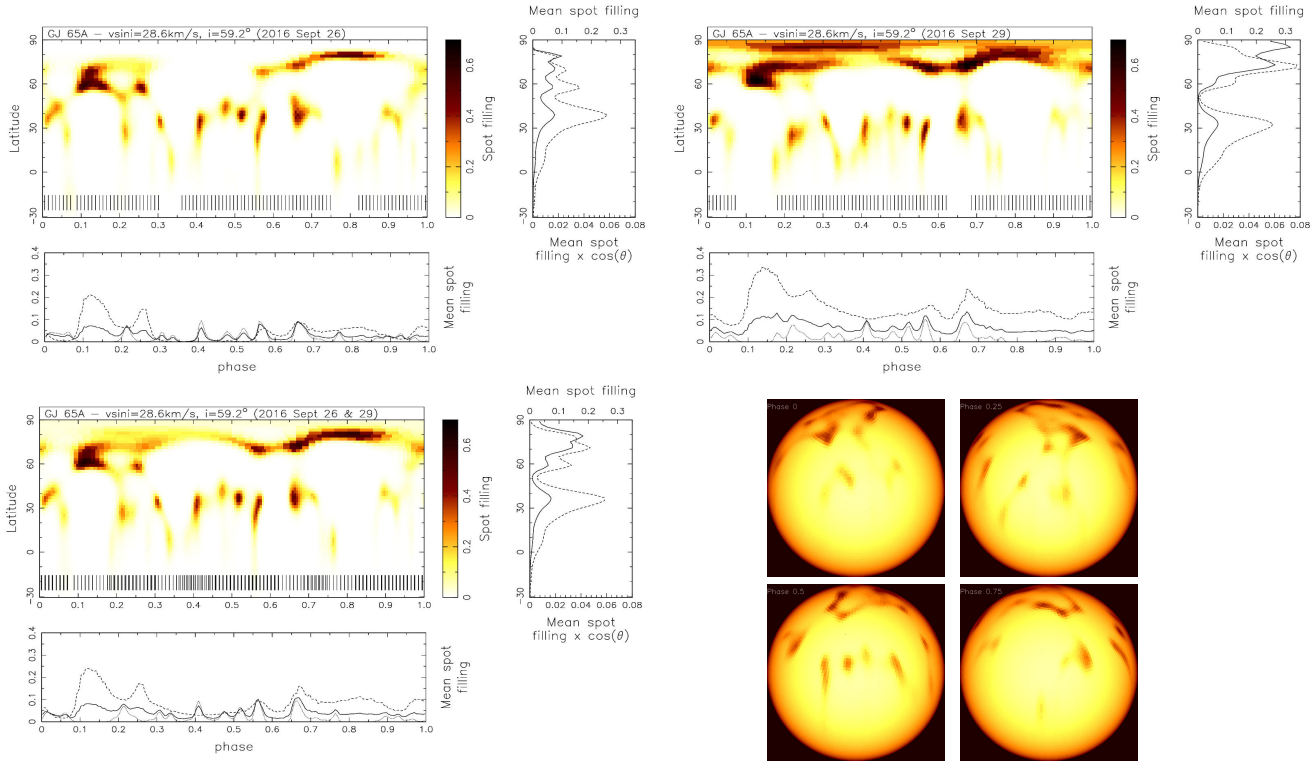

Figure 4: As in Fig. 2 for BL Ceti.

a single high SNR line profile to be derived from the several thousand photospheric absorption lines observed in the 0.38 μm-wide region of each spectrum.

We applied the two-temperature, maximum-entropy regularised imaging algorithm, DoTS (Collier Cameron, 2001) to recover Doppler images of our targets. DoTS uses a spot filling factor, f_i (taking values in the range 0.0 - 1.0), for each image pixel, i. Since the absorption lines present in the spectra of mid-late M stars are dominated by molecular transitions, it isn't immediately clear that a two-temperature model is appropriate for starspot mapping. Synthetic spectra were therefore computed using the BT-Settl model atmospheres of Allard *et al.* (2012) with the WITA code (Gadun & Pavlenko, 1997) which uses opacity sources listed in Pavlenko *et al.* (2007); see also Pavlenko (2014) and Pavlenko & Schmidt (2015). To determine intensity ratios and centre-to-limb variations for the appropriate effective temperatures, the model spectra were treated in the same way as the observed spectra. Further details are given in (Barnes *et al.*, 2015).

4 Results

4.1 HU Del (M4.5V)

HU Del is an M4.5V astrometric binary with a period of 1.4731 ± 0.0008 yrs and a maximum separation of $\sim 0.16''$, although the UVES spectra do not show evidence for the secondary. Montes *et al.* (2001) found this young disk system, at 8.84 pc, does not satisfy Hyades Supercluster membership. We previously determined a period of P = 0.3088 d and $v \sin i$ = 35.1 ± 0.4 kms^{-1} using Doppler imaging techniques applied to observations made in 2014 (Barnes *et al.*, 2015). The observations from 2015 September 25 and 28 secured 59% and 57% phase coverage, giving 33% phase overlap. Compared with the 2014 observations, this improved repeated phase coverage led to revised period and rotation determinations of 0.3427 ± 0.0013 d and $v \sin i$ = 35.3 ± 0.4 kms^{-1}.

The time series spectra presented in Fig. 1 reveal repeated features on both 2015 September 25 and 28 with some possible evolution of starspot features (white trails). A flare occurred at the end of the first night, necessitating adjustment of the mean of the equivalent widths of the affected deconvolved line profiles to the mean of the unaffected profiles. The image combining both nights was derived first (Fig. 2, bottom), and used as a starting image for the individual September 25 (Fig. 2, top) and September 28 (Fig. 2, bottom) images. Thus, reconstruction artefacts of the starspot features at the edge of the phase coverage on each map for the individual nights are minimised. Without sufficient information to constrain the images, regions outside the phase coverage of each individual night will closely resemble the features in the combined nights image and should therefore not be compared in detail.

The reconstructed images in Fig. 2, show a number of spots distributed across the surface of the star, but with evidence for clustering at latitude 15°. A small polar spot is also seen in the 2015 images, but is not present if the 2014 images presented in Barnes *et al.* (2015) where spots are instead seen clustered at high latitudes. The regions of phase overlap show stability between the September 25 and September 28 images, but there is some evidence for spot evolution. A greater degree of spot filling is also found compared with the 2014 images. In 2014, we modelled the spots with intensities corresponding to a temperature difference (in the model atmospheres) of ΔT = 300 K, whereas the 2015 images required ΔT = 400 K (in both instances, we assumed a photospheric temperature of $T_{\rm phot}$ = 3000 K). The respective intensity ratios at disc centre for ΔT = 300 K and 400 K are $I^c_{\rm spot}/I^c_{\rm phot}$ = 0.42 and 0.32. The recovered spot filling factors are 2.7% in the 2015 image and 3.2% in the 2014 image. The filling factors are difficult to compare: in 2015, cooler spots were reconstructed, but using a lower spot temperature (i.e. smaller $I^c_{\rm spot}/I^c_{\rm phot}$ ratio; higher contrast) may be responsible for the lower *mean* spot filling factor.

4.2 BL Ceti (M5.5V)

BL Ceti (GJ 65A) is the brighter component of the visual binary, GJ 65, the 6th closest stellar system to the Sun[2] at 2.68 pc. Montes *et al.* (2001) finds that GJ 65 is a possible member of the 600 Myr Hyades supercluster moving group. Phase coverage on September 26 and 29 of 93% and 89% respectively resulted in 82% phase overlap. The repeating starspot features (Fig. 3) enabled the period to be determined using χ^2 minimisation with DoTS modelling, giving P = 0.2432 ± 0.0006 d. A projected rotation velocity of $v \sin i$ = 28.6 ± 0.3 kms^{-1} and axial inclination of $59 \pm 5^{\rm o}$ are found.

A large number of starspot trails are seen in the time series spectra of BL Ceti in Fig. 3. A remarkable degree of consistency is found in the time series for each of September 26 and 29, separated by three days, or equivalently, >12 stellar rotations. For HU Del, we used $T_{\rm phot}$ = 2800 K and $T_{\rm spot}$ = 2400 K i.e. ΔT = 400 K with an intensity ratio of $I^c_{\rm spot}/I^c_{\rm phot}$ = 0.64. We are able to fit the spectra with $T_{\rm spot}$ = 2500 K (ΔT = 300 K and $I^c_{\rm spot}/I^c_{\rm phot}$ = 0.39), but used $T_{\rm phot}$ = 2400 K to enable a direct comparison with UV Ceti (§4.3 below).

As with BL Ceti, spots are seen distributed at a range of phases (or longitudes) and latitudes with a concentration of low latitude spots centred on latitude 35°. Larger high latitude spots, that may actually be unresolved spot groups, are also seen, and may have evolved in size and number between September 26 and September 29. No polar spot is reconstructed. A mean spot filling of 1.9% is found. Hence despite the numerous spot features, the degree of spot filling is low compared with earlier G and K spectral types (Strassmeier, 2009), and as with HU Del, the contrast ratio required to model the time series spectra is low (c.f. Berdyugina 2005).

4.3 UV Ceti (M6V)

The well known flare star, UV Ceti (GJ 65B), is slightly less massive than its companion; Geyer *et al.* (1988) estimate respective masses of 0.101 $M_\odot$ and 0.099 $M_\odot$. We find P = 0.2269 ± 0.0005 d and $v \sin i$ = 32.0 ± 0.4 kms^{-1}, revealing that UV Ceti is a faster rotator than BL Ceti. An axial inclination of $61 \pm 4^{\rm o}$ is consistent with that found for BL Ceti.

The time series spectra of UV Ceti in Fig. 5 appear similar to those of BL Ceti, but the starspot trails are broader. The first 25 spectra on September 26 were not used because UV Ceti was in a flaring state. Although regions around chromospherically sensitive lines were not use for deconvolution in all stars, the UV Ceti outburst distorted the line profile and continuum shape in the deconvolved profiles, with otherwise unseen He I lines (i.e. λ = 0.66782 μm and 0.70652 μm) appearing in emission. The equivalent width of Hα during the

[2] recons.org

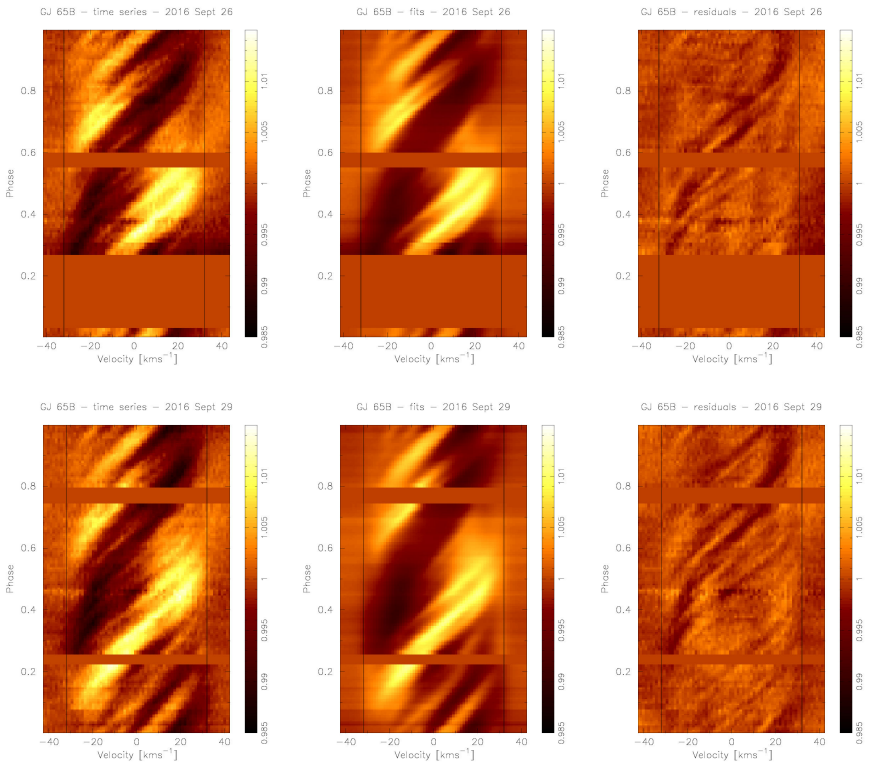

Figure 5: As fin Fig. 1 for UV Ceti (GJ 65B; M6V). $v \sin i$ = 32.0 kms^{-1}.

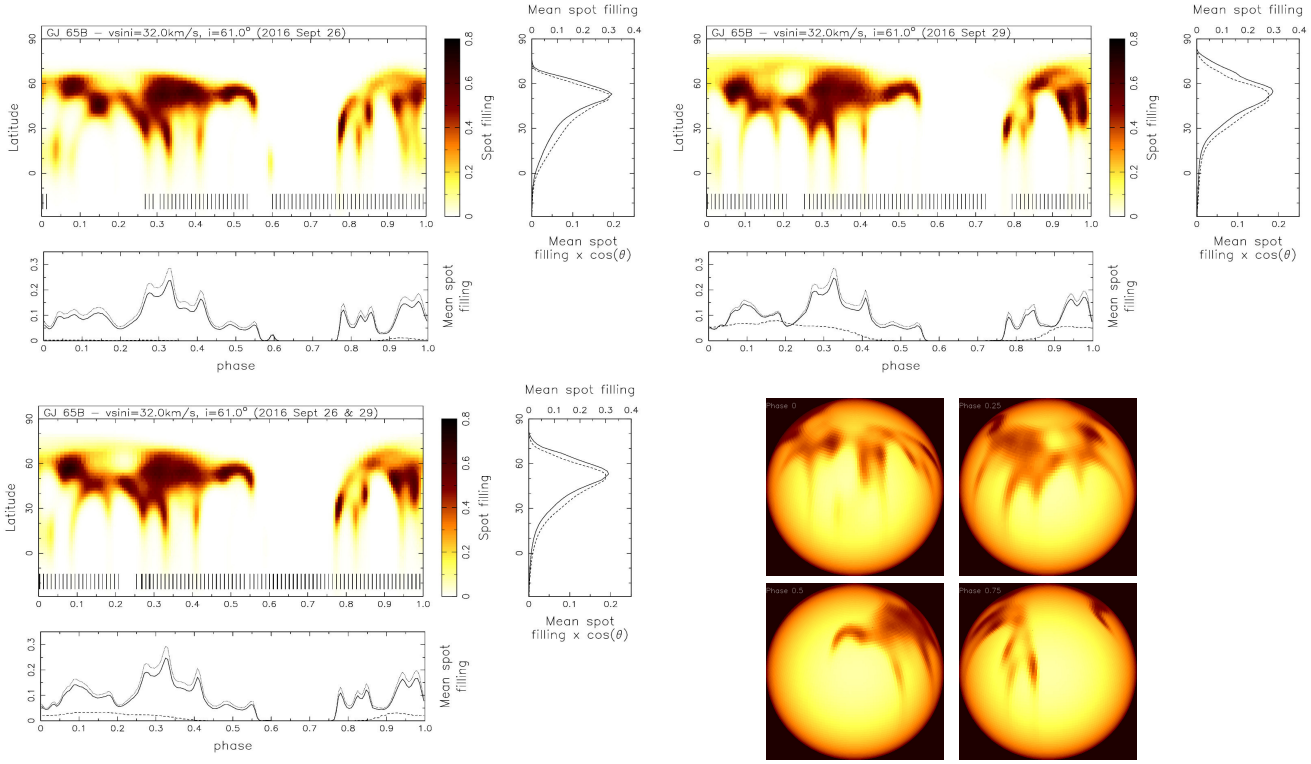

Figure 6: As in Fig. 2 for UV Ceti.

flare event was also >7 times higher than during the quiescence and was clearly visible in the un-extracted spectra. A good fit was obtained using $\Delta T = 400$ K, as with BL Ceti. The reconstructed images in Fig. 6 are nevertheless quite different from those of BL Ceti, with strong spot filling factors located in a region centered on latitude 55^{o}. Individual spots are resolved, but strong filling between the main spot concentrations is seen. Despite good phase coverage, no spots are recovered on either night between phases $\sim$0.56 and $\sim$0.77. No circum-polar structure is recovered. Again, the starspot structure is remarkably stable after three nights ($>$13 rotations). The spot filling factor of 5.3% is somewhat greater than found on either BL Ceti or HU Del.

4.4 Differential rotation

Since the time series spectra and reconstructed images show stable spot structure at both epochs, on September 25/26 and September 28/29, we were able to include differential rotation as a fitting parameter during the modelling. The sheared-image method for obtaining differential rotation was first implemented by Petit *et al.* (2002) and used by Barnes *et al.* (2005) to determine the dependence of differential rotation with spectral type in a number of rapidly rotating G, K and M main sequence stars. The two early M dwarfs in this sample were found to possess differential rotation rates consistent with zero (Barnes *et al.*, 2004, 2005). A solar-like rotation law is adopted, where the rotation rate is a function of the square of the sine of the stellar latitude. Expressed in terms of angular velocity, Ω, the equation for the rotation is

$$\Omega(\theta) = \Omega_{\rm eq} - \Delta\Omega sin^2(\theta) \quad (1)$$

where θ is the stellar latitude, $\Omega_{\rm eq}$ ($= 2\pi/P_{\rm eq}$) is the equatorial rotation rate, and $\Delta\Omega$ is the magnitude of the shear. Barnes *et al.* (2005), found the dependency of shear on rotation to be weak, but instead found a significant trend with stellar temperature, with $\Delta\Omega \propto T_{\rm eff}^{8.9}$. This degree of differential rotation was subsequently revisited by Reiners (2006), incorporating results for F dwarfs using Fourier analysis and further revised by Collier Cameron (2007), who found $\Delta\Omega \propto T_{\rm eff}^{8.6}$.

For HU Del, BL Ceti and UV Ceti, we find differential rotation shear values of $\Delta\Omega = 0.027 \pm 0.067$, 0.051 ± 0.064 and -0.041 ± 0.065; all consistent with zero. We plot our results in Fig. 7 along results for other M dwarfs determined by Morin *et al.* (2008b), Morin *et al.* (2008a) and Donati *et al.* (2008) and the early G dwarf measurement from Marsden *et al.* (2011). The differential rotation is at most relatively weak in fully convective stars, but a weaker dependence of $\Delta\Omega \propto T_{\rm eff}^{6.4\pm1.1}$ is found.

5 Summary

Fully convective M dwarf stars with v sin $i \sim$30 kms^{-1} and rotation periods of a few hours show that starspots are still numerous at the bottom of the main sequence. Starspot coverage of only a few percent is found for all stars, but UV Ceti may be an extreme case, since it is clearly more active than BL Ceti, and shows somewhat different starspot structure to either HU Del or BL Ceti. All images presented here and in Barnes *et al.* (2015) show spots distributed at a range of phases and latitudes, often with evidence of low-latitude bands of spots. However, all stars show significant spots or spot structure at intermediate to high (60^{o} - 90^{o}) latitudes, including the M9V star, LP 944-20, for which we only recover spots at high latitudes. Amongst the latest M dwarfs, the intensity contrast between the photosphere and spots is much smaller than in earlier spectral types, continuing the trend reported by Berdyugina (2005). This is further supported by the observations of LP 944-20, where starspots were recovered with contrast ratios of only $I^c_{\rm spot}/I^c_{\rm phot}$ = 0.64, corresponding to model atmospheres with $\rm T_{phot}$ - $\rm T_{spot}$ = 100 K (Barnes *et al.*, 2015).

Many starspots are stable on timescales of three days suggesting that relatively stable magnetic fields are present. Nevertheless, evolution, including the appearance of new spots, is also seen. It is not clear how the activity seen amongst fast rotators scales to more slowly rotating counterparts, but one might reasonably expect slower rotators to exhibit coherent spot structure on timescales greater than the few days seen here. This has important implications for searches for low-mass planets that are expected in significant numbers around M stars (Tuomi *et al.*, 2014; Dressing & Charbonneau, 2015), with potentially similar orbital periods to the stellar rotation periods.

Acknowledgments

This work is based on observations collected at the European Organisation for Astronomical Research in the Southern Hemisphere under ESO programmes 093.D-0165(A) and 095.D-0291(A). J.R.B. and C.A.H. and M.E.L. were supported by the STFC under the grant ST/L000776/1. S.V.J. acknowledges research funding by the Deutsche Forschungsgemeinschaft (DFG) under grant SFB 963/1, project A16. JSJ acknowledges funding by Fondecyt through grants 1161218 and 3110004, and partial support from CATA-Basal (PB06, Conicyt), the GEMINI-CONICYT FUND and from the Comité Mixto ESO-GOBIERNO DE CHILE.

References

Allard, F., Homeier, D., Freytag, B., & Sharp, C. M. 2012, In *EAS Publications Series*, edited by C. Reylé, C. Charbonnel, & M. Schultheis, *EAS Publications Series*, vol. 57, pp. 3–43.

Barnes, J. R., Cameron, A. C., Donati, J.-F., James, D. J., Marsden, S. C., *et al.* 2005, MNRAS, 357, L1.

Barnes, J. R. & Collier Cameron, A. 2001, MNRAS, 326, 950.

Barnes, J. R., Collier Cameron, A., Unruh, Y. C., Donati, J. F., & Hussain, G. A. J. 1998, MNRAS, 299, 904.

Barnes, J. R., James, D. J., & Cameron, A. C. 2004, MNRAS, 352, 589.

Barnes, J. R., Jeffers, S. V., Jones, H. R. A., Pavlenko, Y. V., Jenkins, J. S., *et al.* 2015, ApJ, 812, 42.

Barnes, J. R., Jenkins, J. S., Jones, H. R. A., Rojo, P., Arriagada, P., *et al.* 2012, MNRAS, 424, 591.

Berdyugina, S. V. 2005, Living Reviews in Solar Physics, 2, 8.

Collier Cameron, A. 2001, In *Astrotomography - Indirect Imaging Methods in Observational Astronomy*, edited by Boffin, H. M. J. and Steeghs, D. and Cuypers, J., pp. 183–206 (Springer (Lecture Notes in Physics)).

Collier Cameron, A. 2007, Astronomische Nachrichten, 328, 1030.

Donati, J., Morin, J., Petit, P., Delfosse, X., Forveille, T., *et al.* 2008, MNRAS, 390, 545.

Donati, J.-F., Semel, M., Carter, B., Rees, D. E., & Collier Cameron, A. 1997, MNRAS, 291, 658.

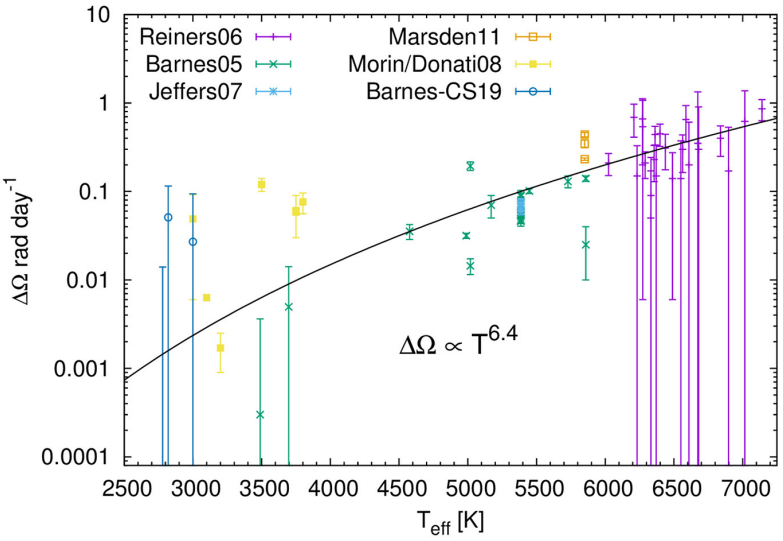

Figure 7: Differential rotation vs stellar effective temperature for stars using the sheared image and Fourier transform methods.

Dressing, C. D. & Charbonneau, D. 2015, ApJ, 807, 45.
Gadun, A. S. & Pavlenko, Y. V. 1997, A&A, 324, 281.
Geyer, D. W., Harrington, R. S., & Worley, C. E. 1988, AJ, 95, 1841.
Johns-Krull, C. M. & Valenti, J. A. 1996, ApJ, 459, L95+.
Marsden, S. C., Jardine, M. M., Ramírez Vélez, J. C., Alecian, E., Brown, C. J., *et al.* 2011, MNRAS, 413, 1922.
Montes, D., López-Santiago, J., Gálvez, M. C., Fernández-Figueroa, M. J., De Castro, E., *et al.* 2001, MNRAS, 328, 45.
Morin, J., Donati, J., Petit, P., Delfosse, X., Forveille, T., *et al.* 2008a, MNRAS, 390, 567.
Morin, J., Donati, J.-F., Forveille, T., Delfosse, X., Dobler, W., *et al.* 2008b, MNRAS, 384, 77.
Pavlenko, Y. V. 2014, Astronomy Reports, 58, 825.
Pavlenko, Y. V., Jones, H. R. A., Martín, E. L., Guenther, E., Kenworthy, M. A., *et al.* 2007, MNRAS, 380, 1285.
Pavlenko, Y. V. & Schmidt, M. 2015, Kinematics and Physics of Celestial Bodies, 31, 90.
Petit, P., Donati, J.-F., & Collier Cameron, A. 2002, MNRAS, 334, 374.
Phan-Bao, N., Lim, J., Donati, J.-F., Johns-Krull, C. M., & Martín, E. L. 2009, ApJ, 704, 1721.
Reiners, A. 2006, A&A, 446, 267.
Saar, S. H. & Linsky, J. L. 1985, ApJ, 299, L47.
Strassmeier, K. G. 2009, The Astronomy and Astrophysics Review, 17, 251.
Tuomi, M., Jones, H. R. A., Barnes, J. R., Anglada-Escudé, G., & Jenkins, J. S. 2014, MNRAS, 441, 1545.